Journal of Catalysis 364 (2018) 183–191

Contents lists available at ScienceDirect

Journal of Catalysis

journal homepage: www.elsevier.com/locate/jcat

PdRu alloy nanoparticles of solid solution in atomic scale: Size effects on electronic structure and catalytic activity towards electrooxidation of formic acid and methanol

Xiongwu Kang [a,*], Kanghua Miao [b], Zhiwei Guo [b], Jiasui Zou [a], Zhenqing Shi [c], Zhang Lin [c], Jie Huang [b,*], Shaowei Chen [a,d]

[a] Guangzhou Key Laboratory for Surface Chemistry of Energy Materials, New Energy Research Institute, School of Environment and Energy, South China University of Technology, Guangzhou 510006, China
[b] Department of Chemical Engineering, Shanxi Key Laboratory of Physico-Inorganic Chemistry, Northwest University, Xi'an, Shanxi 710069, China
[c] Guangdong Engineering and Technology Research Center for Environmental Nanomaterials, School of Environment and Energy, South China University of Technology, Guangzhou, Guangdong 510006, China
[d] Department of Chemistry and Biochemistry, University of California, 1156 High Street, Santa Cruz, CA 95064, United States

ARTICLE INFO

Article history:
Received 4 February 2018
Revised 21 May 2018
Accepted 23 May 2018
Available online 8 June 2018

Keywords:
Alloy nanoparticles
Solid solution in atomic scale
Size effect
Formic acid oxidation
Methanol oxidation

ABSTRACT

It has been challenging to synthesize palladium (Pd) and ruthenium (Ru) alloy nanoparticles of solid solution in atomic scale, thus preventing us to study the size effect on the catalytic activity. Here we reported the synthesis of PdRu alloy nanoparticles through polyol reduction method, with the size from 6.0 to 16.6 nm. Elemental mapping indicated that Pd and Ru with 1:1 ratio are evenly distributed over the alloy nanoparticles. XRD of PdRu alloy nanoparticles displayed the characteristic diffraction patterns of face centered cubic (fcc) of Pd and invariable inter plane distance of (1 1 1). The band width of valence state increased from 5.7 to 6.2 eV when the diameter of the nanoparticles increased from 6.0 to 16.6 nm. The size effect of PdRu alloys towards electrooxidation of formic acid was examined on the support of CNT. PdRu alloy nanoparticles with diameter of 15.6 nm performed best among all the samples, 5.7 times higher than that of commercial Pd/C with formic acid. PdRu alloy nanoparticles also demonstrated optimum catalytic activity towards methanol oxidation in alkaline medium solution and the best performance was achieved by PdRu alloy nanoparticles with diameter of 15.6 nm, which was 2.5 times that of Pd/C. A volcano shape dependence of catalytic activity towards both formic acid and methanol oxidation on the size of PdRu alloy nanoparticles was observed. This work provided a vial strategy for the size-controlled synthesis of alloy nanoparticles of solid solution in atomic scale, especially for those elements that are immiscible, unraveled the size effect on the electronic structure and catalytic activity on metal nanoparticles and may shed light on the optimization of alloy noble metal nanoparticles.

1. Introduction

Proton exchange membrane fuel cells (PEMFCs), the most promising alternative energy source to fossil fuels, have been receiving extensive attentions in the past decades [1–3]. However, the massive commercialization of fuel cells is limited by the high cost and low catalytic activity of the precious noble metal-based catalyst for oxygen reduction reaction on cathode and formic acid oxidation on the anode. Currently, the state-of-the-art catalyst on anode towards formic acid oxidation is maintained by the platinum (Pt) or palladium (Pd)-based catalysts. Compared to Pt, Pd is more cost-effective, free of CO poisoning and thus have become the most promising candidate for anode catalyst [4,5]. Thus far, many efforts have been devoted to further improve the activity and unravel the factors that are dominating the performance of the catalyst. Tuning the size of metal nanoparticles [6,7], alloying with a second metal [8–11] or making inter metallic nanoparticles [12], modulating the strain of the shell metal through core-shell nanostructures [13,14], supported with metal oxide [15,16] and surface engineering [17] of Pd nanomaterials were found to be efficient approaches to improve the catalytic activity towards formic acid oxidation [18]. For example, Zhou and co-workers studied the size effect of the pure Pd nanoparticles and found that the highest activity was achieved by Pd NPs with size of 5–7 nm [19]. Ge

* Corresponding authors.
E-mail addresses: esxkang@scut.edu.cn (X. Kang), huangjie@nwu.edu.cn (J. Huang).

https://doi.org/10.1016/j.jcat.2018.05.022
0021-9517/

et al. [20] reported the sized-controlled synthesis of Pd nanoparticles ranging from 3.1 to 8.1 nm and found that 3.1 nm of Pd nanoparticles are most active towards formic acid oxidation and the catalytic activity of Pd nanoparticles decreases with the increase of nanoparticles size.

PdRu alloy is anticipated to have similar electronic structure and catalytic activity to Rh from the element strategy [21], which demonstrated extremely high catalytic activity but limited by the extremely high cost and rareness. It has been challenging to synthesize PdRu alloy nanoparticles since Pd and Ru are immiscible in atomic level [22]. Until very recently, PdRu alloy nanoparticles of solid solution in atomic scale was synthesized and showed remarkably high activity towards CO and formic acid oxidation [22,23]. However, due to the difficulty of size-controlled synthesis of PdRu alloy nanoparticles of solid solution in atomic scale, size effect of PdRu alloy nanoparticles on the catalytic performance, which is critical parameters in tuning the catalytic activity of metal nanoparticles, remained unexplored yet.

Herein, we synthesized well-dispersed PdRu alloy NPs with the size ranging from 6.0 nm to 16.6 nm. The PdRu alloy nanoparticles were characterized by HRTEM, elemental mapping and X-ray diffraction and the structure of solid solution in atomic scale was confirmed. The bandwidth of valence states was observed to be increasing with the size of the alloy nanoparticles. The size effect on the electro-catalytic activity toward formic acid oxidation was also examined. It was found that PdRu alloy nanoparticles with diameter of 15.6 exhibited the highest catalytic activity and a volcano shape dependence of catalytic activity on the size of PdRu nanoparticles was observed.

2. Experimental

2.1. Chemicals

$Na_2[PdCl_4]$ (99%, Energy Chemical) and $RuCl_3{\cdot}xH_2O$ (99%, J&K), Poly(N-vinyl-2-pyrrolidone) (PVP, MW ≈ 40000, Energy Chemical), triethyleneglycol (TEG, 99%, MACKLIN), Nafion (0.5 wt%, Alfa Aesar), ethanol absolute (99%, DM) and acetone (99%, DM) were used as received. Deionized water was supplied by a Barnstead Nanopure water system (18.3 MΩ cm).

2.2. Synthesis of PdRu alloy nanoparticles

In a typical synthesis [22,23] of PdRu nanoparticles, 444 mg of PVP was dissolved in 100 mL of TEG and the solution was heated to 200 °C in oil bath with magnetic stirring. Meanwhile, 0.5 mmol of $Na_2[PdCl_4]$ and 0.5 mmol of $RuCl_3{\cdot}xH_2O$ were dissolved in 40 mL of water. Such a solution was then slowly added dropwise into the TEG at 200 °C in 40 min. After cooling to room temperature, acetone and alcohol were added into the TEG solution to precipitate the nanoparticles, followed by centrifugation. The precipitation and centrifugation was repeated 5 times to remove unbound PVP. The derived PdRu alloy nanoparticles were denoted as PdRu-4. PdRu alloy nanoparticles of any other sizes were prepared via the same protocol, by adjusting the ratio of Pd^{2+} and Ru^{3+} to PVP, as summarized in Table S1. The as-prepared PdRu alloy nanoparticles were denoted as PdRu-x, (x = 1, 2, 3 and 5).

2.3. Characterization

The powder X-ray diffraction (p-XRD) measurements were carried out on a Bruker D8 diffractometer with Cu Kα radiation (λ = 0.15406 nm). The elemental compositions and valence states of PdRu alloy nanoparticles were examined by X-ray photoelectron spectroscopy (XPS, Phi X-tool instrument). High resolution transmission electron microscopy (HRTEM) images of the nanoparticles were acquired on JEOL TEM-2010 for the analysis of the size distribution. Elemental mapping data was collected on Tecnai G2 F30 of FIE.

2.4. Electrochemical measurements

The catalyst ink was prepared by dispersing CNT and as-prepared PdRu alloy NPs in ethanol successively upon sonication for 1 h and 2 h respectively. The mass ratio of PdRu alloy nanoparticles to CNT was 20: 80. Before casting the catalyst ink, the glassy carbon electrode (GCE, Φ = 6 mm) was polished with 0.3 μm alumina powders on a polishing microcloth for 20 min and successive sonication in sulfuric acid solution (3 M) and ultra-pure water for 10 min respectively. The electrode surface was then cleaned under UV irradiation for 15 min for any potential organic contaminants. Subsequently, 10 μL catalyst ink (1 mg/ml) was cast on GCE prepared above and dried under air flux at room temperature, followed by deposition of 5 μL of Nafion (0.5 wt%) on top of the nanoparticles and natural evaporation in air. The electrochemical characterization was conducted on a CHI 650E electrochemical workstation (CH Instruments Inc.), with a conventional three-electrode system at room temperature (25 °C). The alloy PdRu nanoparticles-coated GCE was used as the working electrode, a Hg/Hg_2Cl_2 with saturated KCl solution as the reference electrode and a Pt slice as counter electrode. The cyclic voltammetry was performed at a scan rate of 100 mV s^{-1} and the electrochemical surface area (ECSA) was determined from the hydrogen under potential deposition (H_{upd}) region in 0.5 M perchloric acid aqueous solution [19] and the reduction of palladium oxide in 1 M NaOH aqueous solution [24]. The catalytic activity of alloy PdRu nanoparticles towards formic acid oxidation and stability test were carried out in 0.5 M formic acid in 0.5 M perchloric acid solution at a scan rate of 50 mV s^{-1}. The CO stripping was investigated in 0.5 M perchloric acid solution at ascan rate of 5 mV s^{-1}. Initially, the 0.5 M perchloric acid solution was degassed with N_2 for 20 min and bubbled with CO for 5 min, in which the chronoamperometric (CA) measurement was acquired at 0.2 V (vs SCE). Upon CA measurement finished and CO bubbling stopped, the solution was degassed again by N_2 again for 20 min and 2 cycles of CV were acquired with a scan rate of 5 mV s^{-1}. Methanol oxidation was measured in 1 M methanol in 1 M NaOH aqueous solution with scan rate of 50 mV s^{-1}.

3. Results and discussion

The size of PdRu alloy nanoparticles were modulated by changing the ratio of metal precursor to PVP surfactant. As shown in Fig. 1, PdRu-x (x = 1, 2, 3, 4 and 5) alloy NPs were well-dispersed. The mean diameters of the nanoparticles were determined to be (A) 16.6 ± 0.4, (B) 15.6 ± 0.3, (C) 9.3 ± 0.5, (D) 7.7 ± 0.4, and (E) 6.0 ± 0.3 nm for PdRu-x (x = 1, 2, 3, 4 and 5), respectively, suggesting the size-controlled synthesis of PdRu alloy nanoparticles. The histograms of size distribution for PdRu alloy nanoparticlesare shown in Fig. S1. From the HRTEM images in the insets of Fig. 1(A)–(E), the lattice spacing of PdRu alloy nanoparticles of all sizes are measured to be 0.223 nm. Consistent with Xia [25] and Stamenkovic's [26] report, the inter plane distance of alloy nanoparticles remain intact when the size of PdRu alloy nanoparticles increased. The inter plane distance of PdRu (1 1 1) is slightly smaller than that of Pd (1 1 1) (0.225 nm), attributed to the atomic size of Ru (0.134 nm) is smaller than that of Pd (0.137 nm) and also the formation of PdRu solid solution in atomic scale. The formation of solid solution in atomic scale of PdRu alloy nanoparticles of all sizes was further confirmed by high angle annular dark field (HAADF) and elemental mapping. Fig. 1(F)–(I) shows HAADF image and elemental mapping data for PdRu nanoparticles with diameter of 15.6 nm (PdRu-1),

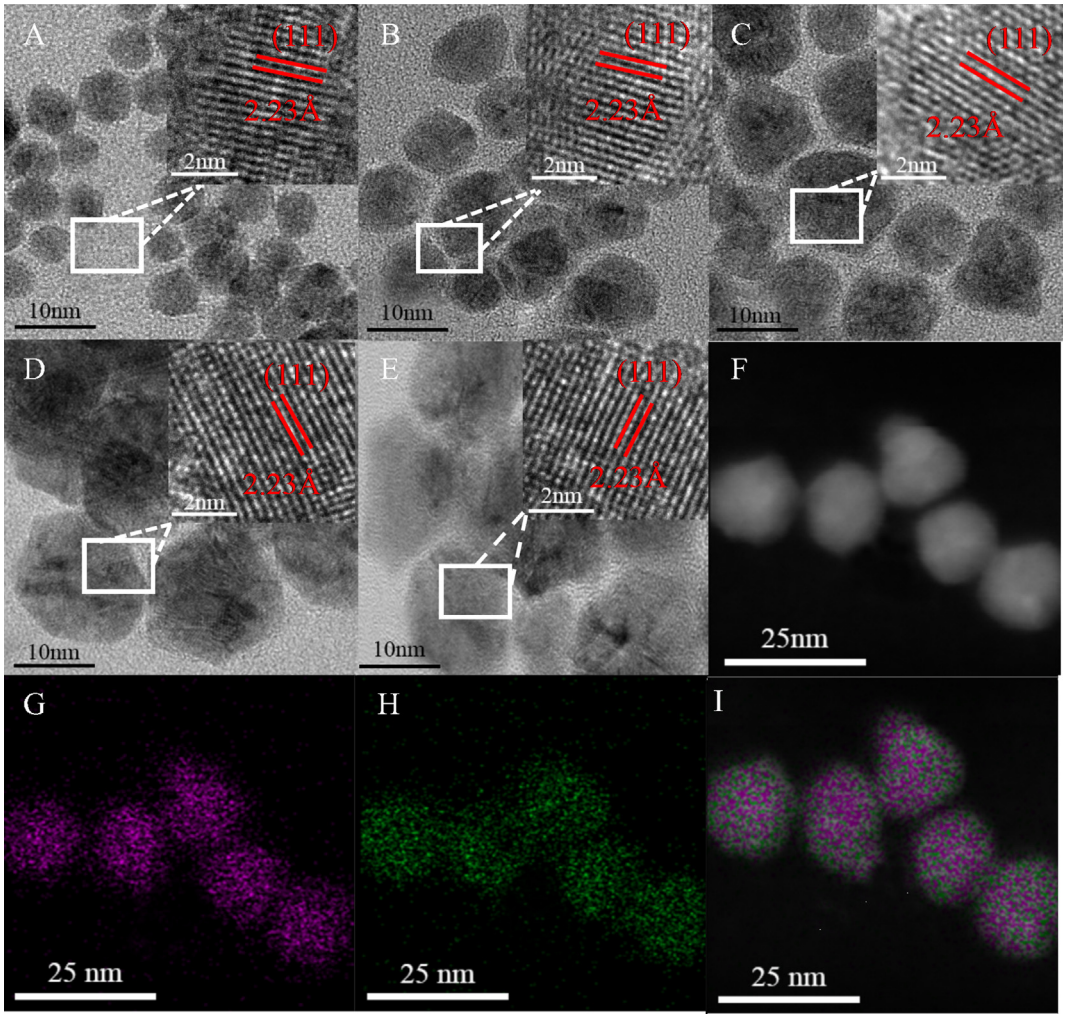

Fig.1. The TEM and HRTEM images of (A) PdRu-1 (d = 6.0 ± 0.3), (B) PdRu-2 (d = 7.7 ± 0.4), (C) PdRu-3 (d = 9.3 ± 0.5), (D) PdRu-4 (d = 15.6 ± 0.3), and (E) PdRu-5 (d = 16.6 ± 0.4) nanoparticles (top inset: HRTEM and lattice planes of Pd(1 1 1) in A–E). (F) HAADF-STEM image, (G) Pd-L and (H) Ru-L and (I) overlap of Pd-L and Ru-L STEM–EDX mapping obtained for PdRu-4 nanoparticles.

where Pd and Ru elements homogeneously distributed all over the nanoparticle, with the ratio of 48.2–51.8, very close to the 1:1 stoichiometric ratio. Similar results were also observed for PdRu-x (x = 1, 2, 3 and 5) alloy nanoparticles. As shown in Fig. 2 and Table S1, Pd and Ru uniformly distributed over the nanoparticles with 1:1 ratio, indicating the formation of solid solution in atomic scale of PdRu alloy nanoparticles of all five samples of different diameters.

The size modulation and the nucleation and growth dynamics of PdRu alloy nanoparticles can be described by LaMer's mechanism [27], which proposed a fast and homogenous "burst nucleation" at some critical and super saturation of the reduced metal precursor and further a slow and diffusion-controlled growth. In the case of this paper, the reducing agent of TEG is excessive in the reaction system and all the metal precursors of Pd and Ru are completely reduced concurrently. Thus the alloy metal nanoparticles nucleation is rapidly formed and then grow slowly. In the presence of protective agent, the diffusion-controlled growth of nanoparticles is limited by the passivation of metal particles' surface by the protectant. When the molar ratio of the PVP to the metal precursor is low, the surface passivation of nanoparticles would be slow and large nanoparticles would be obtained. In contrast, with increased ratio of PVP to metal precursor, the surface passivation of nanoparticles by PVP becomes faster, continuous growth of metal nanoparticles would be stopped in earlier stage and smaller nanoparticles would be made. Concurrent reduction of Pd and Ru precursors, fast nucleation and continuous growth of LaMer's mechanism guaranteed the synthesis of PdRu alloy nanoparticles of solid solution in atomic scale. The size dependence of PdRu alloy nanoparticles to the ratio of PVP to metal precursor are shown in Fig. S2.

The crystallographic structures of PdRu alloy nanoparticles were investigated by XRD measurements, as depicted in Fig. 3. The well-defined face centered cubic (fcc) was observed for all PdRu alloy nanoparticles of different sizes and the diffraction peaks for PdRu alloy nanoparticles were attributed to (1 1 1), (0 0 2), (0 2 2), (3 1 1) and (2 2 2) facets respectively. Based on Bragg's equation, the (1 1 1) inter plane distances of PdRu alloy nanoparticles were calculated to be 2.23 Å, in agreement with that derived from HRTEM results. In agreement with earlier report by Xia [25] and Stamenkovic [26], when the diameter of PdRu alloy nanoparticles increases from 6.0 to 16.6 nm, the inter plane distance of the alloy nanoparticles was consistent with each other while the diffraction peak of PdRu (1 1 1) becomes sharper and narrower, signifying the increased crystalline size.

The binding energy of Pd, a reflection of d band center of Pd metal, is reported to be critical for the catalytic activity of Pd nanoparticles [4,19]. For this purpose, the high resolution XPS spectra of Pd and Ru 3d of PdRu alloy nanoparticles were measured

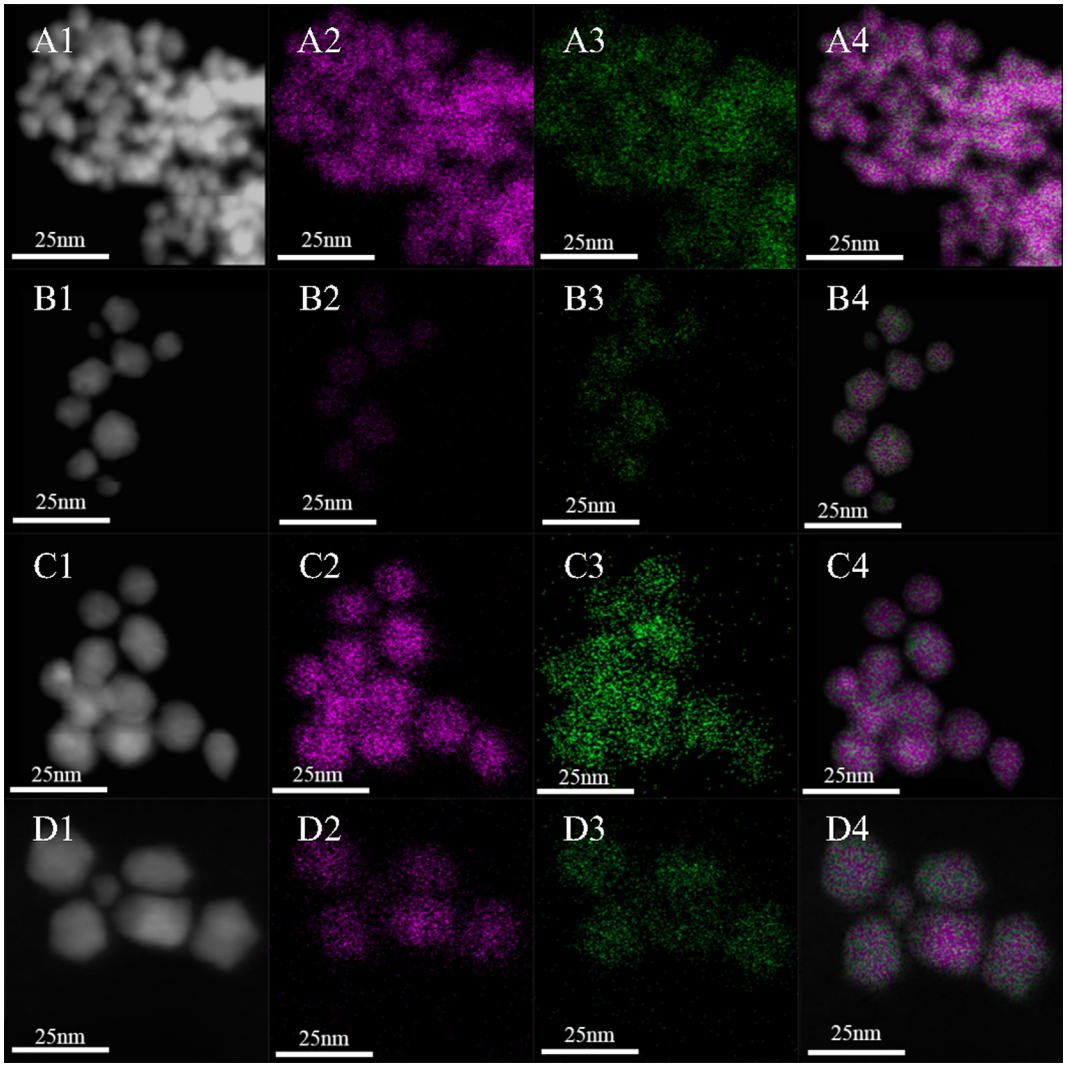

Fig. 2. Pd-L(purple), Ru-L(green) and overlap of Pd-L and Ru-L STEM–EDX mapping obtained for (A) PdRu-1, (B) PdRu-2, (C) PdRu-3 and (D) PdRu-5 nanoparticles.

and depicted in Fig. 4 and Fig. S5. It can be seen that the binding energy of Pd 3d only slightly reduced by 0.2 eV while that of Ru 3d are also very consistent with each other when the size of the nanoparticles increased from 6.0 to 16.6 nm. Fig. 4(B) showed the dependence of bandwidth of valence states (VB) spectra of PdRu alloy nanoparticles derived from Fig. S3, which increases from 5.7 to 6.2 eV when the diameter of PdRu alloy nanoparticles increased from 6.0 to 16.6 nm, in agreement with results observed for Pd nanoparticles in the earlier report.[28,29] The broad peak observed in Fig. S4 (A) at 8 eV might be associated with the formation of PdH on PdRu alloy nanoparticles [30]. In addition, XPS shows that the ratio of Pd to Ru for all samples is close to 1:1, the same as the ratio of the precursor of Pd and Ru used in the synthesis of PdRu alloy nanoparticles (Table S2).

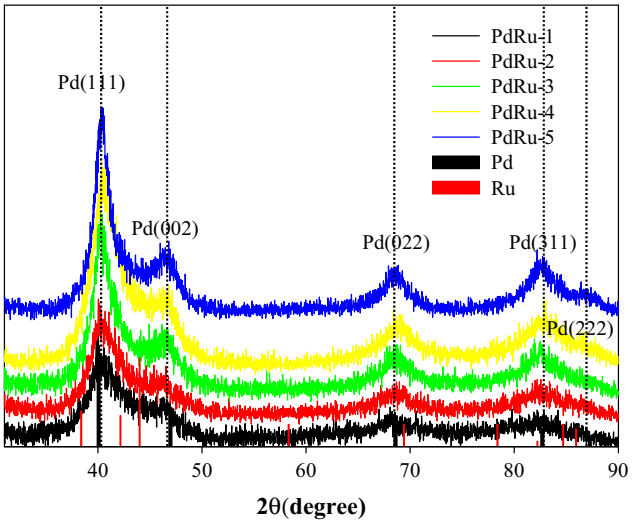

Fig. 3. XRD patterns of PdRu-x (x = 1, 2, 3, 4 and 5) nanoparticles.

Fig. 5(A), (C) and (E) showed the CV scans of PdRu-x/CNT and Pd/C in 0.5 M $HClO_4$ solution at a potential scan rate of 100 mV s^{-1} at room temperature. The currents have been normalized to the unit mass of Pd loadings. The current between −0.25 and 0.0 V can be ascribed to the adsorption/desorption of hydrogen and perchlorate on the Pd surfaces, as well as the absorption of a small fraction of hydrogen into the Pd lattice [31,32]. A well-defined cathodic peak at around +0.35–+0.4 V was attributed to the reduction of Pd oxide that was formed in the anodic scan. The ECSA of the PdRu/CNT nanoparticles was estimated from the hydrogen desorption and listed in Table 1. The ECSA for PdRu-4/CNT was derived to be 28.8 $m^2 g^{-1}$, about 43.0% less than that of Pd/C (50.5 $m^2 g^{-1}$). The ECSA of the PdRu-1 is extremely low, which is only 5 $m^2 g^{-1}$.

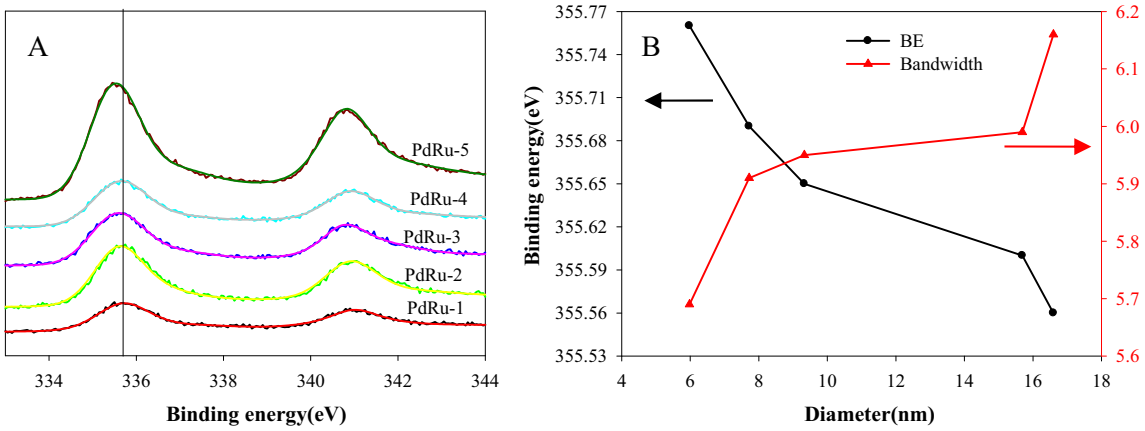

Fig. 4. (A) High resolution XPS spectrum for Pd 3d of PdRu-x alloy NPs, (x = 1, 2, 3, 4 and 5) and (B) dependence of the binding energy (BE) and bandwidth on the diameter of the PdRu alloy nanoparticles.

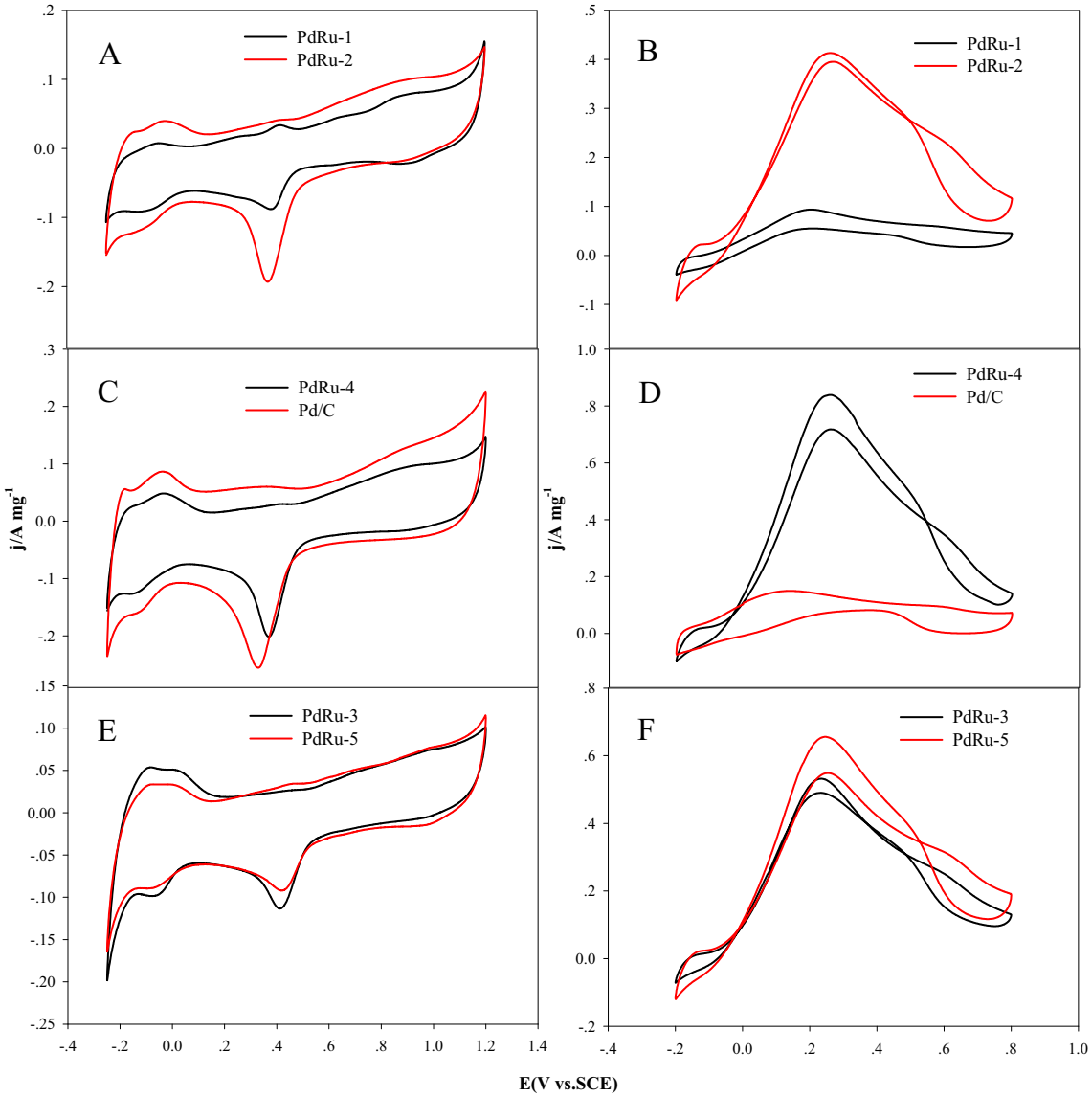

Fig. 5. CVs of PdRu-x and Pd/C in 0.5 M aqueous $HClO_4$ with potential scan rate of 100 mV s^{-1} (A, C, E) and aqueous 0.5 M $HClO_4$ + 0.5 M HCOOH with potential scan rate of 50 mV s^{-1} (B, D, F), with the currents normalized to the unit mass loading of Pd.

Table 1
The ECSA and j_{max} of PdRu alloy nanoparticles towards formic acid oxidation in 0.5 M $HClO_4$ + 0.5 M HCOOH derived from Fig. 5.

Samples	Pd/C	PdRu-1	PdRu-2	PdRu-3	PdRu-4	PdRu-5
d (nm)		6.0 ± 0.3	7.7 ± 0.4	9.3 ± 0.5	15.6 ± 0.3	16.6 ± 0.4
ECSA ($m^2\ g^{-1}$)	50.5	5	24.5	32.3	28.8	19.4
j_{max} ($A\ mg^{-1}$)	0.15	0.10	0.42	0.56	0.85	0.65
j_{max} ($mA\ cm^{-2}$)	0.3	2.0	1.7	1.7	3.0	3.4

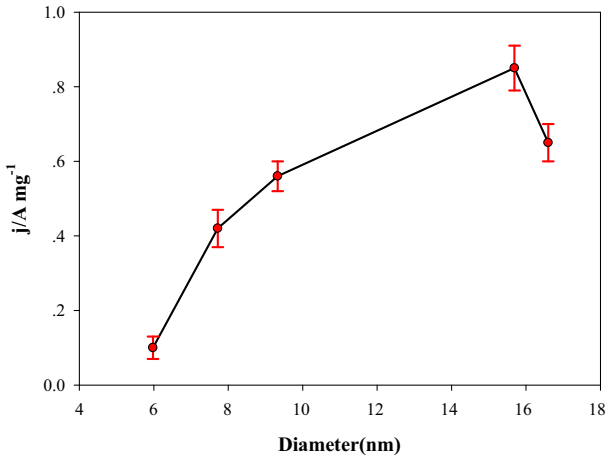

Fig. 6. Dependence of the mass activity of PdRu alloy nanoparticles towards formic acid oxidation on the diameter of PdRu alloy nanoparticles.

This might be ascribed to the formation of PdH on the surface of PdRu-1 alloy nanoparticles, which lead to reduced ECSA determined by hydrogen adsorption [33].

Fig. 5(B), (D) and (F) depicted the CV of the PdRu/CNT and Pd/C catalysts recorded in a 0.5 M HCOOH in 0.5 M $HClO_4$ aqueous solution at a potential scan rate of 50 mV s^{-1} and the normalized peak current density were listed in Table 1. Normally, the increase of the size of the metal nanoparticles leads to the reduced surface area. However, the ECSA of PdRu alloy nanoparticles showed a volcano shape dependence on the size of the PdRu nanoparticles, with the maximum achieved at the size of 9.3 nm (Fig. S6). This might be partially ascribed to the formation of metal hydrides for PdRu alloy nanoparticles, which reduces the ECSA, especially for PdRu nanoparticles of smaller size [33]. As shown in Fig. S4, PdRu-1 (6.0 nm) showed the most obvious hydrides feature in XPS measurement and thus the smallest ECSA. This might account for that abnormal increasing of the ECSA with increase of size for nanoparticles of size ranging from 6.0 to 9.3 nm. In addition, larger PdRu alloy nanoparticles have fewer features of metal hydride and thus

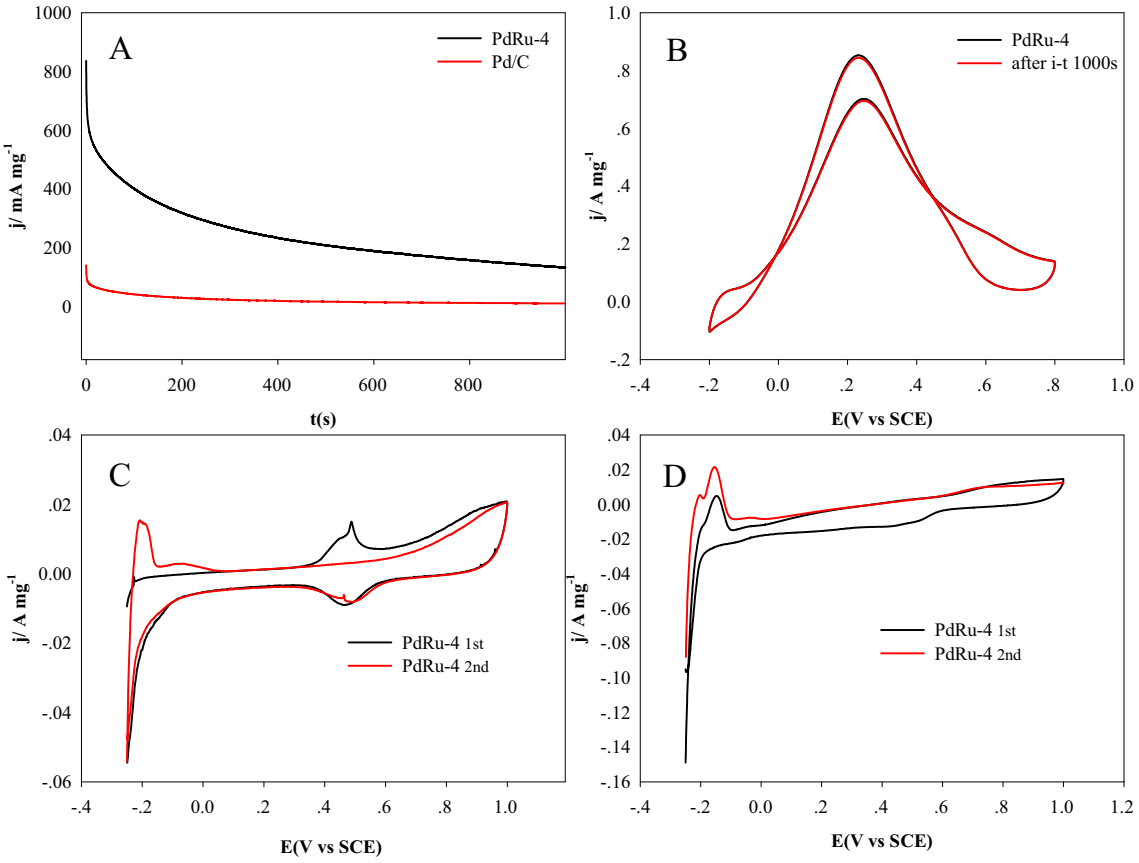

Fig. 7. (A) CA measurements for Pd/C and PdRu alloy nanoparticles with diameter of 15.6 nm; (B) CV of PdRu-4 before and after CA measurement of 1000 s; (C) 1st and 2nd CV scans of PdRu-4 in 0.5 M $HClO_4$, with potential scan rate of 5 mV s^{-1} in the absence of CO after CA measurement for 5 min and in the presence of CO and (D) 1st and 2nd CV scans of PdRu-4 after chronoamperometric measurement of 1000 s in 0.5 M $HClO_4$ + 0.5 M HCOOH, potential scan rate of 5 mV s^{-1}.

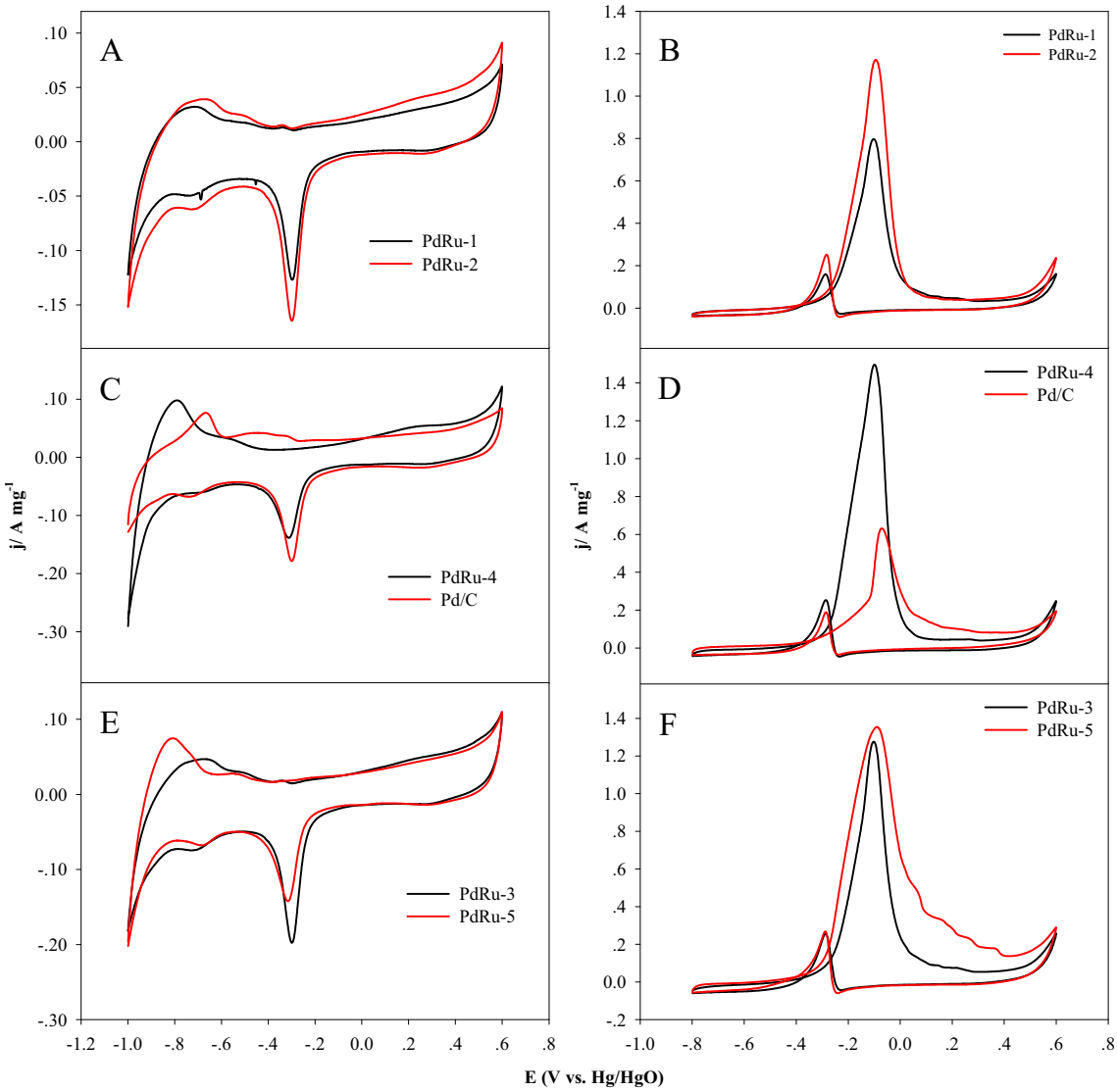

Fig. 8. CV of PdRu alloy nanoparticles and Pd/C in 1 M NaOH solution with potential scan rate of 100 mV s^{-1} (A, C, E) and 1 M CH_3OH in 1 M NaOH with potential scan rate of 50 mV s^{-1} (B, D, F), with the currents normalized to the unit mass loading of Pd metal.

Table 2
The ECSA and j_{max} of PdRu alloy nanoparticles towards methanol oxidation in 1 M NaOH and 1 M methanol in 1 M NaOH solution derived from Fig. 8.

Samples	Pd/C	PdRu-1	PdRu-2	PdRu-3	PdRu-4	PdRu-5
d (nm)		6.0 ± 0.3	7.7 ± 0.4	9.3 ± 0.5	15.6 ± 0.3	16.6 ± 0.4
ECSA ($m^2\ g^{-1}$)	51.7	31.9	44.3	53.8	48.1	45.9
j_{max} (A mg^{-1})	0.63	0.80	1.17	1.28	1.50	1.36
j_{max} (mA cm^{-2})	1.22	2.51	2.64	2.38	3.12	2.96

decreased ECSA with the increase of the size of the alloy nanoparticles (9.3–15.3 nm) was observed, thus resulting in a volcano-shape dependence of ECSA on the size of the alloy nanoparticles was observed.

It can be seen that the catalytic activity of PdRu alloy nanoparticles towards formic acid oxidation is strongly related to the size of the PdRu alloy nanoparticles [4,19,34,35]. The current density increased with the increase of the size of the alloy nanoparticles and maximum current was achieved by PdRu nanoparticles with diameter of 15.6 nm, which is 5.7 times higher than that of Pd/C (0.15 A mg_{Pd}^{-1}). Further increasing the size of PdRu alloy nanoparticles to 16.6 nm, the current density was reduced slightly and a volcano shape dependence of catalytic activity towards formic acid oxidation on the size of PdRu nanoparticles was observed, as shown in Fig. 6. PdRu/CNT alloy nanoparticles with the diameter of 6.0 nm, displayed minimum activity 0.1 A mg_{Pd}^{-1}. Such low catalytic activity might be ascribed to the low ECSA and also the formation of palladium hydrides, as demonstrated in Fig. S4 [30]. Based on the mass activity and the ECSA, the specific activity of PdRu-x alloy nanoparticles of diverse size and Pd/C was calculated and listed in Table 1. It can be seen that the specific activity of PdRu-x is much larger than that of commercial Pd/C and the largest specific activity of PdRu-x

was maintained by largest PdRu alloy nanoparticles of PdRu-5, which is almost 11 times that of Pd/C.

Fig. 7(A) shows the CA profiles of Pd/C and PdRu-4/CNT with the potential at 0.2 V. CA measurements of other samples are shown in Fig. S6. The initial high currents, caused by the combination of formic acid oxidation and double-layer charging, quickly decayed and reached steady state probably due to the adsorption of poisoning intermediates [36,37]. CV scans before and after CA measurement of 1000 s were almost identical to each other, as depicted in Fig. 7 (B), indicating that the activity of catalyst was able to be recovered after CA measurement and the catalyst itself was stable. In other words, the decay of the current in CA measurement resulted from the poisoning intermediates of the formic acid oxidation, instead of the degradation of the catalyst itself. To verify if the attenuation of the catalyst activity was due to the CO_{ads} poisoning [38], two CV scans after CA measurements were conducted in the presence of CO or in formic acid solution respectively, as shown in Fig. 7(C) and (D). Fig. 7(C) shows the results from voltammetric CO stripping using a PdRu4/CNT nanoparticle in 0.5 M $HClO_4$ at 5 mV/s. In the first scan, the CO oxidation peak was observed at 0.48 V (vs SCE) and no hydrogen adsorption feature was observed. However, in the second scan, the characteristic hydrogen adsorption features was recovered while the anodic peak at 0.48 V was gone, suggesting that the adsorbed CO was stripped in the first CV scan and clean Pd surface was recovered. In contrast, no such features were observed for PdRu-4/CNT samples after CA measurement for formic acid oxidation, as shown in Fig. 7(D), suggesting that the current attenuation in CA measurement in Fig. 7(A) for PdRu-4/CNT was not caused by carbon monoxide poisoning, but some other unknown organic intermediates formed during the formic acid oxidation reaction [39]. To test the cycling stability of the catalyst itself, PdRu-4 catalyst was scanned by 1000 cycles in the potential range of −0.2 to 0.8 V at a scanning rate of 50 mV s^{-1} in 0.5 M formic acid in 0.5 M aqueous perchloric acid solution, as shown in Fig. S7. It was observed that the mass activity of carbon black supported PdRu-4 catalyst was attenuated by 17.6%, probably due to the reconstruction of the catalyst surface structure.

The catalytic activity of PdRu alloy nanoparticles towards methanol oxidation in alkaline medium was examined and compared with the commercial Pd/C, as shown in Fig. 8 and Table 2. Due to the formation of the metal hydrides, a volcano-shape dependence of the ECSA of PdRu alloy nanoparticles was observed and the specific activity showed increasing trend with the increase of the PdRu alloy nanoparticles, as shown in Fig. S8(A), which are 1.95–2.55 times higher than that of Pd/C. In addition, the mass activity of PdRu alloy nanoparticles towards methanol oxidation increase with the size of PdRu alloy nanoparticles and achieved the best performance with diameter of 15.6 nm, with the mass activity of 1.50 A mg^{-1}, which is 2.5 times that of Pd/C. Further increase of the size of PdRu alloy nanoparticles resulted in the slight decrease of catalytic activity to 1.36 A mg^{-1}. The dependence of the mass catalytic activity of PdRu-x alloy nanoparticles towards methanol oxidation on the size of the nanoparticles is shown in Fig. S8(B), where volcano-shape dependence was observed. The CA of PdRu-x was measured at −0.1 V in 1 M methanol in 1 M NaOH, which are much more stable than Pd/C (Fig. S9).

4. Conclusions

By following Lamer's mechanism, PdRu alloy nanoparticles of solid solution in atomic scale were prepared and the size of the alloy nanoparticles was tuned by the ratio of Pd and Ru precursor to PVP. HRTEM images, XRD analysis, elemental mapping and XPS measurement confirmed the formation of PdRu alloy nanoparticles in atomic scale. The inter plane distance of PdRu alloy nanoparticles remained constant while the bandwidth of PdRu increased from 5.7 to 6.2 eV when the size of the alloy nanoparticles increased from 6.0 to 16.6 nm. The best performance of the electrocatalytic activity towards formic acid and methanol oxidation was demonstrated by PdRu alloy nanoparticles of 15.6 nm and a volcano shape dependence of the catalytic activity on the size of PdRu nanoparticles was observed.

5. Notes

The authors declare no competing financial interest.

Acknowledgments

This work was supported by the National Natural Science Foundation of China (No. 51602106), the Fundamental Research Funds for Central Universities (SCUT Grant No. 2017MS066) and Technology Research and Development Program of Shanxi Province, China (No. 14JF025). Prof. Z. L. would like to thank the Guangdong Innovative and Entrepreneurial Research Team Program (No. 2016ZT06N569).

Appendix A. Supplementary material

Supplementary data associated with this article can be found, in the online version, at https://doi.org/10.1016/j.jcat.2018.05.022.

References

[1] J.P. Lai, S.J. Guo, Design of ultrathin pt-based multimetallic nanostructures for efficient oxygen reduction electrocatalysis, Small 13 (2017).
[2] P.T. Wang, X. Zhang, J. Zhang, S. Wan, S.J. Guo, G. Lu, J.L. Yao, X.Q. Huang, Precise tuning in platinum-nickel/ nickel sulfide interface nanowires for synergistic hydrogen evolution catalysis, Nat. Commun. 8 (2017).
[3] K.Z. Jiang, D.D. Zhao, S.J. Guo, X. Zhang, X. Zhu, J. Guo, G. Lu, X.Q. Huang, Efficient oxygen reduction catalysis by subnanometer Pt alloy nanowires, Sci. Adv. 3 (2017).
[4] W.P. Zhou, A. Lewera, R. Larsen, R.I. Masel, P.S. Bagus, A. Wieckowski, Size effects in electronic and catalytic properties of unsupported palladium nanoparticles in electrooxidation of formic acid, J. Phys. Chem. B 110 (2006) 13393–13398.
[5] H. Miyake, T. Okada, G. Samjeské, M. Osawa, Formic acid electrooxidation on Pd in acidic solutions studied by surface-enhanced infrared absorption spectroscopy, Phys. Chem. Chem. Phys. 10 (2008) 3662–3669.
[6] C. Wang, D.P. Chen, X. Sang, R.R. Unocic, S.E. Skrabalak, Size-dependent disorder-order transformation in the synthesis of monodisperse intermetallic PdCu nanocatalysts, ACS Nano 10 (2016) 6345–6353.
[7] L. Gan, S. Rudi, C.H. Cui, M. Heggen, P. Strasser, Size-controlled synthesis of sub-10 nm $PtNi_3$ alloy nanoparticles and their unusual volcano-shaped size effect on ORR electrocatalysis, Small 12 (2016) 3189–3196.
[8] M.-H. Shao, K. Sasaki, R.R. Adzic, Pd– Fe nanoparticles as electrocatalysts for oxygen reduction, J. Am. Chem. Soc. 128 (2006) 3526–3527.
[9] D. Wang, H.L. Xin, H. Wang, Y. Yu, E. Rus, D.A. Muller, F.J. DiSalvo, H.D. Abruña, Facile synthesis of carbon-supported Pd–Co core–shell nanoparticles as oxygen reduction electrocatalysts and their enhanced activity and stability with monolayer Pt decoration, Chem. Mater. 24 (2012) 2274–2281.
[10] F. Gao, D.W. Goodman, Pd–Au bimetallic catalysts: understanding alloy effects from planar models and (supported) nanoparticles, Chem. Soc. Rev. 41 (2012) 8009–8020.
[11] S. Zhang, Ö. Metin, D. Su, S. Sun, Monodisperse AgPd alloy nanoparticles and their superior catalysis for the dehydrogenation of formic acid, Angew. Chem. Int. Ed. 52 (2013) 3681–3684.
[12] Z.Y. Qi, C.X. Xiao, C. Liu, T.W. Goh, L. Zhou, R. Maligal-Ganesh, Y.C. Pei, X.L. Li, L. A. Curtiss, W.Y. Huang, Sub-4 nm PtZn intermetallic nanoparticles for enhanced mass and specific activities in catalytic electrooxidation reaction, J. Am. Chem. Soc. 139 (2017) 4762–4768.
[13] M.B. Gawande, A. Goswami, T. Asefa, H.Z. Guo, A.V. Biradar, D.L. Peng, R. Zboril, R.S. Varma, Core-shell nanoparticles: synthesis and applications in catalysis and electrocatalysis, Chem. Soc. Rev. 44 (2015) 7540–7590.
[14] M. Luo, S. Guo, Strain-controlled electrocatalysis on multimetallic nanomaterials, Nat. Rev. Mater. 2 (2017) 17059.
[15] Z. Xi, J. Li, D. Su, M. Muzzio, C. Yu, Q. Li, S. Sun, Stabilizing CuPd nanoparticles via CuPd coupling to $WO_{2.72}$ nanorods in electrochemical oxidation of formic acid, J. Am. Chem. Soc. 139 (2017) 15191–15196.
[16] Y.Z. Lu, Y.Y. Jiang, X.H. Gao, X.D. Wang, W. Chen, Strongly coupled Pd nanotetrahedron/tungsten oxide nanosheet hybrids with enhanced catalytic

activity and stability as oxygen reduction electrocatalysts, J. Am. Chem. Soc. 136 (2014) 11687–11697.
[17] Z.-Y. Zhou, X. Kang, Y. Song, S. Chen, Butylphenyl-functionalized palladium nanoparticles as effective catalysts for the electrooxidation of formic acid, Chem. Commun. 47 (2011) 6075–6077.
[18] S. Alayoglu, P. Zavalij, B. Eichhorn, Q. Wang, A.I. Frenkel, P. Chupas, Structural and architectural evaluation of bimetallic nanoparticles: a case study of Pt-Ru core-shell and alloy nanoparticles, ACS Nano 3 (2009) 3127–3137.
[19] W.J. Zhou, J.Y. Lee, Particle size effects in Pd-catalyzed electrooxidation of formic acid, J. Phys. Chem. C 112 (2008) 3789–3793.
[20] J. Ge, W. Xing, X. Xue, C. Liu, T. Lu, J. Liao, Controllable synthesis of Pd nanocatalysts for direct formic acid fuel cell (DFAFC) application: from Pd hollow nanospheres to Pd nanoparticles, J. Phys. Chem. C 111 (2007) 17305–17310.
[21] E. Nakamura, K. Sato, Managing the scarcity of chemical elements, Nat. Mater. 10 (2011) 158–161.
[22] K. Kusada, H. Kobayashi, R. Ikeda, Y. Kubota, M. Takata, S. Toh, T. Yamamoto, S. Matsumura, N. Sumi, K. Sato, K. Nagaoka, H. Kitagawa, Solid solution alloy nanoparticles of immiscible Pd and Ru elements neighboring on Rh: changeover of the thermodynamic behavior for hydrogen storage and enhanced CO-oxidizing ability, J. Am. Chem. Soc. 136 (2014) 1864–1871.
[23] K. Miao, Y. Luo, J. Zou, J. Yang, F. Zhang, L. Huang, J. Huang, X. Kang, S. Chen, PdRu alloy nanoparticles of solid solution in atomic scale: outperformance towards formic acid electro-oxidation in acidic medium, Electrochim. Acta 251 (2017) 588–594.
[24] Y.C. Zhao, L. Zhan, J.N. Tian, S.L. Nie, Z. Ning, Enhanced electrocatalytic oxidation of methanol on Pd/polypyrrole-graphene in alkaline medium, Electrochim. Acta 56 (2011) 1967–1972.
[25] S.I. Choi, S. Xie, M. Shao, N. Lu, S. Guerrero, J.H. Odell, J. Park, J. Wang, M.J. Kim, Y. Xia, Controlling the size and composition of nanosized Pt–Ni octahedra to optimize their catalytic activities toward the oxygen reduction reaction, Chemsuschem 7 (2014) 1476–1483.
[26] C. Wang, D. van der Vliet, K.-C. Chang, H. You, D. Strmcnik, J.A. Schlueter, N.M. Markovic, V.R. Stamenkovic, Monodisperse Pt_3Co nanoparticles as a catalyst for the oxygen reduction reaction: size-dependent activity, J. Phys. Chem. C 113 (2009) 19365–19368.
[27] V.K. LaMer, R.H. Dinegar, Theory, production and mechanism of formation of monodispersed hydrosols, J. Am. Chem. Soc. 72 (1950) 4847–4854.
[28] G. Wertheim, S. DiCenzo, D. Buchanan, Noble-and transition-metal clusters: the d bands of silver and palladium, Phys. Rev. B 33 (1986) 5384.
[29] M. Mason, L. Gerenser, S.-T. Lee, Electronic structure of catalytic metal clusters studied by X-ray photoemission spectroscopy, Phys. Rev. Lett. 39 (1977) 288.
[30] P. Bennett, J. Fuggle, Electronic structure and surface kinetics of palladium hydride studied with x-ray photoelectron spectroscopy and electron-energy-loss spectroscopy, Phys. Rev. B 26 (1982) 6030.
[31] N. Hoshi, K. Kagaya, Y. Hori, Voltammograms of the single-crystal electrodes of palladium in aqueous sulfuric acid electrolyte: Pd (S)-[n (111)×(111)] and Pd (S)-[n (100)×(111)], J. Electroanal. Chem. 485 (2000) 55–60.
[32] H. Duncan, A. Lasia, Separation of hydrogen adsorption and absorption on Pd thin films, Electrochim. Acta 53 (2008) 6845–6850.
[33] Z. Zhao, X. Huang, M. Li, G. Wang, C. Lee, E. Zhu, X. Duan, Y. Huang, Synthesis of stable shape-controlled catalytically active β-palladium hydride, J. Am. Chem. Soc. 137 (2015) 15672–15675.
[34] X. Ji, K.T. Lee, R. Holden, L. Zhang, J. Zhang, G.A. Botton, M. Couillard, L.F. Nazar, Nanocrystalline intermetallics on mesoporous carbon for direct formic acid fuel cell anodes, Nat. Chem. 2 (2010) 286–293.
[35] S. Park, Y. Xie, M.J. Weaver, Electrocatalytic pathways on carbon-supported platinum nanoparticles: comparison of particle-size-dependent rates of methanol, formic acid, and formaldehyde electrooxidation, Langmuir 18 (2002) 5792–5798.
[36] J. Bao, M. Dou, H. Liu, F. Wang, J. Liu, Z. Li, J. Ji, Composition-dependent electrocatalytic activity of palladium-iridium binary alloy nanoparticles supported on the multiwalled carbon nanotubes for the electro-oxidation of formic acid, ACS Appl. Mater. Int. 7 (2015) 15223.
[37] Z. Liu, X. Zhang, S.W. Tay, Nanostructured PdRu/C catalysts for formic acid oxidation, J. Solid State Electrochem. 16 (2012) 545–550.
[38] Y.Z. Lu, W. Chen, One-pot synthesis of heterostructured Pt-Ru nanocrystals for catalytic formic acid oxidation, Chem. Commun. 47 (2011) 2541–2543.
[39] X. Yu, P.G. Pickup, Recent advances in direct formic acid fuel cells (DFAFC), J. Power Sour. 182 (2008) 124–132.